

Definition of Static and Dynamic Load Models for Grid Studies of Electric Vehicles Connected to Fast Charging Stations

Davide del Giudice, *IEEE Member*, Angelo Maurizio Brambilla, *IEEE Member*, Federico Bizzarri, *IEEE Senior Member*, Daniele Linaro, *IEEE Member*, Samuele Grillo, *IEEE Senior Member*

Abstract—The growing deployment of electric mobility calls for power system analyses to investigate to what extent the simultaneous charging of electric vehicles leads to degraded network operation and to validate the efficiency of countermeasures. To reduce complexity and CPU time, a common approach while performing these analyses consists in replacing electric vehicles and their charging stations with constant PQ loads. However, this approach is inaccurate, as the power absorbed by these elements actually depends not only on voltage but also on the state of charge, charging method, cathode chemistry of the battery pack, and converter controls in the electric vehicle and charging station.

By considering all these aspects, this article develops a novel static load model and a vector fitting-based dynamic load model for electric vehicles connected to fast charging stations. These computationally efficient representations can replace the standard constant PQ load model of electric vehicles to assess more accurately their impact in static and dynamic grid studies. Simulation results of the IEEE14 system modified by adding fleets of electric vehicles prove the accuracy of the proposed models and highlight the shortcomings of the standard electric vehicle representation as a constant PQ load in some cases.

Index Terms—Electric vehicles, fast charging stations, load modelling, static load model, dynamic load model, vector fitting, power system analysis, small-signal stability

I. INTRODUCTION

ELECTRIC mobility is growing at a staggering pace. In 2021, the global fleet of electric vehicles (EVs) exceeded 16.5 million, which was three times the amount in 2018. This trend is envisaged to intensify, culminating in the sale of around 200 million EVs by 2030 [1]. However, despite reducing greenhouse gas emissions, the rising popularity of electric mobility challenges modern power systems. Indeed, unless properly managed, adverse effects of massive EV deployment include larger voltage drops and losses, grid overloads, and a decrease in power quality [2], [3].

A vast literature has been produced to analyze these phenomena and consequently develop mitigating measures that allow postponing or at least minimizing the need for grid reinforcement operations [4]. A popular solution consists in implementing delayed or controlled charging strategies [5]. These solutions are usually validated through power flow analyses based on a probabilistic approach. For example, in the case of *mobility-aware* charging strategies, probability density functions are used to describe EVs charging time, location,

duration, as well as their state of charge (SoC) before charging [6], [7]. While these aspects have been studied at considerable length, relatively less attention has been paid to the derivation of an equivalent EV load model, which is just as essential to accurately assess the impact of electric mobility on the grid.

In principle, for this purpose one might resort to detailed EV models that allow analysing electrical variables at the converter level. However, this would lead to prohibitive CPU times and a degree of accuracy that is typically excessive for large-scale power system simulations. On the opposite side of the complexity spectrum, most of the previously mentioned studies reduce EVs to mere constant active and reactive power (PQ) loads [8]. This simplification is in line with [9], according to which about 70% of utilities and system operators worldwide rely on PQ load models for steady-state power system studies. Such a modelling approach has become common practice because it is easy to implement, has a low computational burden, and generally implies considering a worst-case scenario, thereby providing results that are well within safety boundaries [10], [11].

Nonetheless, there are some exceptions arguing that the constant PQ load model does not adequately reflect the real behaviour of EVs, not even at steady-state. In the context of static load modelling, the works in [12] and [13] describe EVs with a ZIP model by adopting a measurement-based approach. Other works resort to a *multistage* ZIP model, where piecewise functions describe the EV active and reactive power exchange; each interval is defined by different ZIP model parameters and represents a specific EV working condition (e.g., charging time [14] or SoC [15], [16]). Lastly, [17] employs an exponential model, extended to the multistage version in [18], [19].

Concerning EV dynamic load modelling, the existing literature is limited. The works in [20]–[22] include early attempts to perform stability analyses of networks with EVs by analytically developing a small-signal model. However, analyses are restricted to simple grids comprising one generator and an EV described by models of different degrees of detail. A dynamic model was developed in [23] by simulating voltage disturbances at the EVs point of connection and fitting their power transient with a first-order response. However, as the authors of [23] acknowledge, this model does not always adequately represent EVs: indeed, based on the control parameters of the converters in the EVs and charging stations (CSs), the order of the dynamic response may be higher than one.

In this work, we propose accurate and computationally efficient static and dynamic load models of EVs connected to fast CSs, which can replace the standard representation as

D. del Giudice, S. Grillo, F. Bizzarri, D. Linaro, and A.M. Brambilla are with Politecnico di Milano, DEIB, p.zza Leonardo da Vinci, n. 32, 20133 Milano, Italy. (e-mails: {name.surname}@polimi.it).

Italian MIUR project PRIN 2017K4JZEE_006 funded the work of S. Grillo (partially) and D. del Giudice (totally).

constant PQ loads to assess more precisely the impact of rising EV penetration during power system studies. Specifically, the contributions of this article are the following.

- A novel static load model is developed that mirrors the dependence of EV power exchange on SoC, voltage, charging method, and the cathode chemistry of the battery pack. This last aspect is novel since previous works usually adopted Li-ion batteries without explicitly stating their cathode chemistry. In this work, we used some of the most popular ones [24], [25]: Lithium Iron Phosphate (LFP), Lithium Manganese Oxide (LMO), Nickel Manganese Cobalt Oxide (NMC), and Nickel Cobalt Aluminum Oxide (NCA).
- A novel dynamic load model based on vector fitting is proposed to describe the dynamic response of EVs during voltage disturbances. The shape of this response mirrors the controls installed in the converters of EVs and their CSs.
- Simulation results during static and dynamic grid studies of the IEEE14 system modified by adding loads given by EV fleets are reported to validate the proposed models and highlight the inaccuracy introduced in some cases by the EV representation as a constant PQ load.

II. OVERVIEW OF STATIC AND DYNAMIC LOAD MODELS

The next subsections outline some load models that are helpful for better understanding those proposed in this work. In general, a load model describes the relationship between the voltage and power at the bus where the load is connected. For static and dynamic load models, this relationship is respectively given by algebraic and differential equations [26].

A. Static load models

The most popular static load representations are the polynomial (ZIP) and exponential (EXP) [27] models, which relate load active power exchange P to voltage magnitude v as

$$P_{\text{ZIP}} = P_{\text{nom}} \left(k_0 + k_1 \left(\frac{v}{v_{\text{nom}}} \right) + k_2 \left(\frac{v}{v_{\text{nom}}} \right)^2 \right) \quad (1)$$

$$P_{\text{EXP}} = P_{\text{nom}} \left(a_p + b_p \left(\frac{v}{v_{\text{nom}}} \right)^{n_p} \right), \quad (2)$$

where P_{nom} is the load active power at nominal voltage v_{nom} (analogous formulas hold for the reactive power Q). Based on the values of k_0 , k_1 , and k_2 , the ZIP model can synthesize constant power/current/impedance loads (or a mixture of those). As opposed to ZIP representation, the EXP model can correctly reproduce also loads like air-conditioning systems [28], which are potentially detrimental to grid stability as their power absorption is inversely proportional to v (i.e., $n_p < 0$). In these cases, using ZIP models could lead to inaccurate power system analyses. Other representations improve the above ones by adding terms that mirror the power dependence on frequency [11] and resorting to multistage models [29].

B. Dynamic load models

Dynamic load models extend static representations and allow describing load behaviour during voltage disturbances.

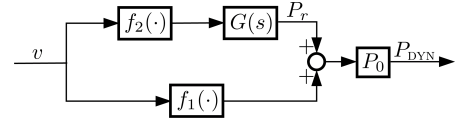


Fig. 1. General block structure representation of the dynamic load model.

The models outlined hereafter can be implemented through the schematic in Fig. 1. The active power exchange is

$$P_{\text{DYN}} = P_0 (f_1(v) + P_r) = P_0 (f_1(v) + G(s)f_2(v)), \quad (3)$$

where P_0 refers to the power exchange before any disturbance occurs (an analogous formula holds for the reactive power). The P_r term is the power recovery part and mirrors the power transient undergone by the load immediately after a voltage disturbance and before reaching a new steady-state value. The functions $f_1(v)$, $f_2(v)$ and the transfer function $G(s)$ give shape to this transient and their expression depends on the specific dynamic model used. In the literature, several formulations were developed, such as the exponential recovery load model (ERLM), oscillatory component load model (OCLM), and vector fitting-based load model (VFLM).

The ERLM describes a first-order response and is one of the oldest dynamic load representations. It was originally introduced to describe how on load tap changers (OLTCs) connected to loads influenced dynamic power system behaviour [30]. In principle, the ERLM can be readapted to model the dynamics of other loads possibly lacking OLTCs but falls short when higher-order responses need to be mimicked. For instance, this is the case of power electronics interfaced loads, whose P_r component includes an exponential and a damped oscillatory part. To address this issue, one can resort to the OCLM and VFLM [31], [32]. The former models a second-order response, while the latter can describe responses of any order through vector fitting (VF)—an algorithm that approximates a measured or calculated frequency domain response with a rational transfer function $G(s)$ ¹.

In the specific case of the VFLM, the expressions of $f_1(v)$, $f_2(v)$, and $G(s)$ are the following

$$\begin{aligned} f_1(v) &= \left(\frac{v}{v_0} \right)^{N_t} \\ f_2(v) &= \left(\frac{v}{v_0} \right)^{N_s} - \left(\frac{v}{v_0} \right)^{N_t} \\ G(s) &= \sum_{n=1}^{N_p} \frac{c_n}{s - a_n} \end{aligned} \quad (4)$$

where v_0 is the load voltage before any disturbance occurs, and N_p is the number of poles used with VF to describe $G(s)$, whose poles and residues are a_n and c_n , respectively. The work in [31] explains the procedure required to derive $G(s)$ and the unknown parameters of this model (i.e., N_t , N_s , c_n , and a_n), which is not repeated here for the sake of brevity.

¹The interested reader is referred to [33]–[35] for details about this algorithm and to [36] for a downloadable VF software package.

III. ELECTRIC VEHICLE AND CHARGING STATION MODEL

The development of static and dynamic EV load models requires executing three preliminary steps: (i) the identification of the EV and CS components that need to be modelled, (ii) the definition of the control scheme used to regulate EV charging, and (iii) the selection of adequate topology and control parameters that reflect realistic EVs and CSs. Each of these phases is addressed in the next subsections.

A. EV and CS topology

When parked for charging, the most relevant elements of the EV are the battery pack and the charger, while the traction drive, motor, and other mechanical parts are neglected. Based on the application, the charger is either on-board or off-board the EV. They are respectively suitable for a slow charge (e.g., through a household power outlet) and fast charge (i.e., through a dedicated CS). This work focuses on fast CSs. Figure 2 depicts an implementation example: the charger consists of a two-stage AC-DC/DC-DC power conversion [12], while the battery pack comprises $N_{\text{cell,par}}$ parallel branches of $N_{\text{cell,ser}}$ series-connected identical cells [37].

The different blocks of Fig. 3 depict the average model of the CS in the AC and DC sides (including the cells in the EV battery pack) adopted in this work. The variables highlighted in red are the output of the EV charging control architecture described in the following, while those associated with a wavy arrow denote the active or reactive power at a given point.

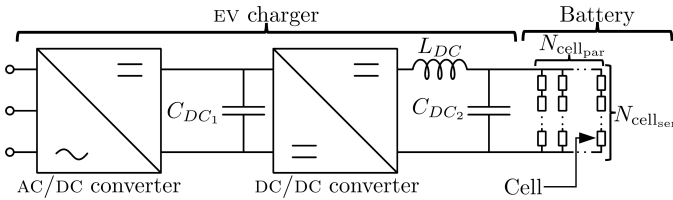


Fig. 2. Synthetic schematic of the main components of an EV and its CS.

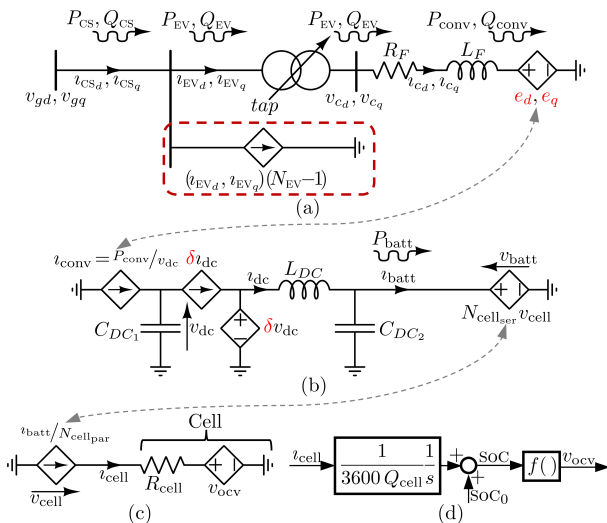


Fig. 3. Schematic of the CS and EV at AC side (a) and DC side (b), single cell in a battery pack (c), the i_{cell} -OCV relationship of a single cell (d). Dashed double arrows denote coupling between the dependent sources.

Figure 3(a) describes the AC side of the AC/DC converter through a single-phase schematic in the DQ frame (ignore for now the circuit in the dashed section, whose purpose is explained in section IV). It includes an R_F - L_F filter and an e_d - e_q dependent voltage source. An ideal transformer with adjustable tap ratio is added to the CS to serve a twofold purpose. First, it facilitates the connection of CSs to any bus of the benchmark system used in the following (which may operate at different nominal voltages) by selecting a proper transformation ratio. Second, by changing its tap ratio during power flow and transient simulations, it allows investigating EV behaviour and deriving static and dynamic load models—an approach commonly used also for other loads [31].

As shown in Figure 3(b), the DC side of the AC/DC converter is given by a dependent current source that acts as an ideal power coupler between the two sides of the converter. The two dependent sources δi_{dc} and δv_{dc} (together with C_{DC1} , C_{DC2} , and L_{DC}) implement the average model of the DC/DC converter described in [38]. Lastly, a dependent voltage source mirrors the voltage given by the series connection of $N_{\text{cell,ser}}$ cells, which are assumed to behave in the same way.

Figure 3(c) depicts the model of a single cell. The current dependent source relates the cell and battery currents (i.e., i_{cell} and i_{batt}) through the number of parallel branches $N_{\text{cell,par}}$. The single cell can be described through models of different degrees of accuracy [39]. In this work, the cell comprises an equivalent series resistance R_{cell} and a dependent voltage source which imposes the open circuit voltage (OCV). In turn, as shown in Fig. 3(d), this voltage depends on the cell's SoC and current through a non-linear relationship $f(\cdot)$. In [40], [41], this relationship is approximated by

$$f = v_{\text{ocv}}(\text{SoC}_0) = E_0 - K \frac{1 - \text{SoC}_0}{\text{SoC}_0} Q + A e^{(1 - \text{SoC}_0) Q}, \quad (5)$$

where Q and SoC_0 are respectively the capacity and initial SoC of the whole battery pack, while E_0 , K , and A are specific cell parameters that vary with the chemistry of the cell.

In this work, rather than resorting to analytical expressions, we used the OCV-SoC relationships of the Li-ion cathode chemistries cited in the introduction and shown in Fig. 4, which have been obtained by interpolating the experimental results reported in Fig. 6 of [42].

B. CS control architecture

The two converters in the CS used in this work are entrusted with different tasks. As shown in Fig. 5(a), the AC/DC converter implements vector current control and exploits variables formulated in the DQ frame [43]. It is in charge of keeping

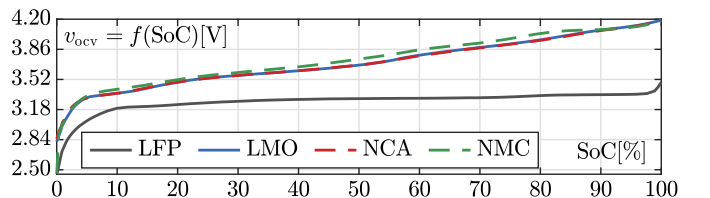


Fig. 4. OCV-SoC relationship of the Li-ion cell chemistries considered [42].

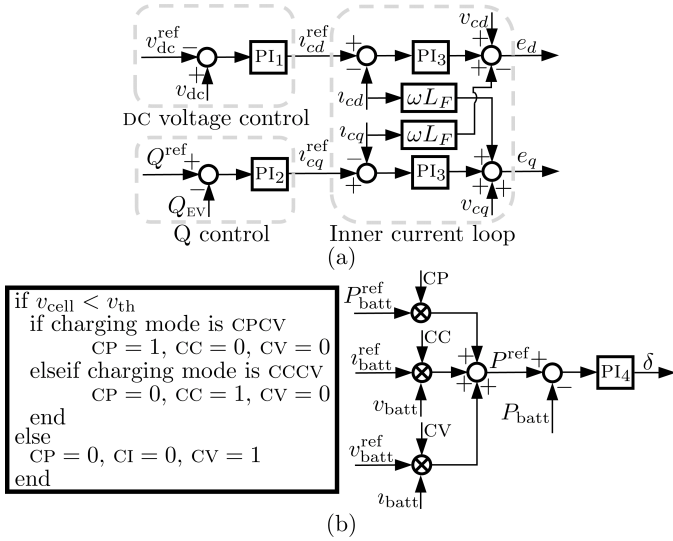


Fig. 5. Control architecture of the AC/DC (a) and DC/DC (b) converters.

the voltage v_{dc} across the capacitor C_{DC1} close to the value v_{dc}^{ref} and ensuring that the EV exchanges no reactive power Q_{EV} (i.e., power factor correction is implemented and, thus, $Q^{ref} = 0$). These control loops define a reference value for the current i_c (see Fig. 3(a) for its location) on the direct and quadrature axis, which are translated by an inner current loop into the e_d, e_q components of the dependent voltage source.

Figure 5(b) depicts the DC/DC converter control scheme. Its purpose is to regulate the duty cycle δ of the converter so that the power absorbed by the battery pack matches a reference value P^{ref} . This value is defined according to the pseudo-code in Fig. 5(b), which controls the battery based on the charging mode employed (i.e., either Constant Current Constant Voltage (CCCV) or Constant Power Constant Voltage (CPCV)) and the difference between the cell voltage v_{cell} and a given threshold v_{th} [37]. During charge, one variable at a time among P_{batt} , i_{batt} , and v_{batt} (see Fig. 3(b) for their locations) is regulated to follow a reference value denoted by the superscript ref . In turn, as shown in Fig. 5(b), these variables determine P^{ref} .

C. EV and CS specifics

To accurately assess the impact of rising electric mobility on the grid, the synthesis of equivalent static and dynamic load models must stem from a realistic design of EVs and CSs.

In this regard, in the simulations described in the following sections, we considered fast CSs of $P_{EV,nom} = 50$ kW nominal power (a value compatible with [2]) and the 2017 Tesla Model S as reference EV, given by a $E_{EV,nom} = 75$ kWh battery [44] and an assumed nominal DC voltage of $V_{EV,nom} = 400$ V.

As to the cathode chemistry of the Li-ion battery pack (information rarely disclosed by EV manufacturers), we selected those cited in the introduction, associated with the data in Table I [42]. For each of them, the number of series-connected cells and parallel branches equals respectively $N_{cell,ser} = \text{round}\left(\frac{V_{EV,nom}}{v_{cell,nom}}\right)$ and $N_{cell,par} = \text{round}\left(\frac{E_{EV,nom}}{V_{EV,nom} Q_{cell}}\right)$, with Q_{cell} being the nominal cell capacity.

TABLE I
ELECTRIC VEHICLE AND CHARGING STATION DATA

Battery cell parameters				
Chemistry	$v_{cell,nom}$ [V]	Q_{cell} [Ah]	R_{cell} [Ω]	v_{th} [V]
LFP	3.20	2.6	0.053	3.488
LMO	3.70	2.6	0.080	4.188
NCA	3.60	3.2	0.058	4.188
NMC	3.60	2.0	0.080	4.183
Charging station parameters				
R_F [m Ω]	L_F [mH]	C_{DC1} [mF]	L_{DC} [mH]	C_{DC2} [mF]
3.20	0.2	1	0.2	0.5
Control reference values				
v_{dc}^{ref} [V]	Q^{ref} [VAR]	P_{batt}^{ref} [kW]	v_{batt}^{ref} [V]	i_{batt}^{ref} [A]
800	0	50	$N_{cell,ser} v_{th}$	$\frac{P_{batt}^{ref}}{v_{batt}^{ref}}$
PI regulator parameters				
	PI ₁	PI ₂	PI ₃	PI ₄
k_p	0.01	0	0.142	0.001
k_i	1000	33	43.909	1

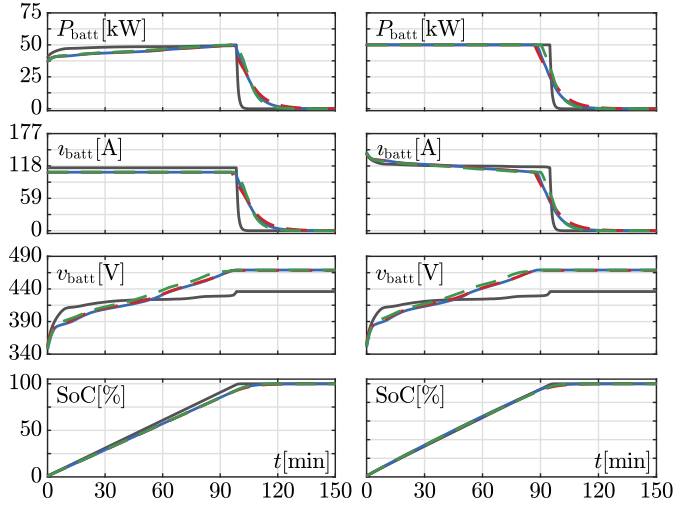


Fig. 6. From top to bottom: evolution of P_{batt} , i_{batt} , v_{batt} , and SoC for the benchmark EV with CCCV (left panels) and CPCV (right panels) charging modes and different Li-ion chemistries. Curves are colour-coded as in Fig. 4.

Lastly, the remaining parameters in Table I were used to design the CS and its control architecture. Figure 6 shows the evolution of some battery variables obtained with the abovementioned design during a full EV charge (i.e., from 0 to 100% SoC) for each chemistry and charging mode.

IV. SIMULATION RESULTS

In this section, computationally efficient and accurate static and dynamic load models of EVs are developed by using as a benchmark the IEEE14 power system, whose parameters can be found in [45]². The obtained models are also used for static and dynamic grid studies involving fleets of EVs, as shown in Fig. 7. Such analyses prove that the proposed models allow gathering results comparable to those obtained with detailed EV representations and highlight the inaccuracy introduced in some cases by modelling EVs as simple constant PQ loads.

²The simulation results shown hereafter were obtained with PAN simulator [46]–[48]. The files needed to run the simulations are available on GitHub at https://github.com/Davide-del-Giudice/Electric_vehicle_models.git

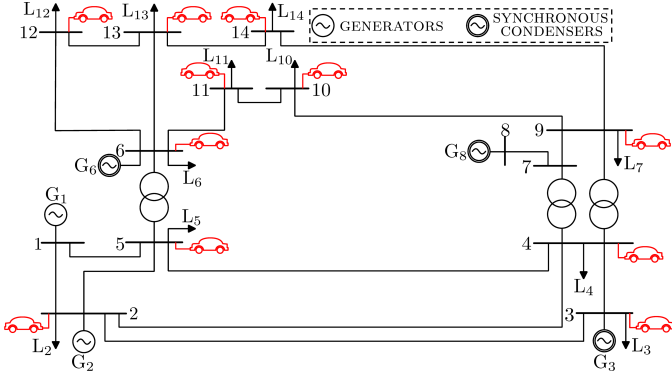


Fig. 7. The schematic of the modified IEEE14 power system with EV fleets.

A. Static EV load model derivation

We first simulated the charge of a single EV through a fast CS in different cases. In each case, we considered one of the previously mentioned cell chemistries, charging modes, and a set of initial SoC values (i.e., SoC_0) ranging from 10 to 90%. By acting on the tap of the transformer in Fig. 3(a), we varied the AC-side voltage magnitude at the point of connection of the AC/DC converter (hereafter referred to as v_c) around its rated value $v_{c,\text{nom}} = \sqrt{v_{c,d}^2 + v_{c,q}^2} = 230$ V and recorded the EV active power normalized with respect to $P_{EV,\text{nom}} = 50$ kW.

So doing, the results in Fig. 8 were obtained (neglect for now the solid lines). Analogous plots for the reactive power are not shown since power factor correction is implemented (thus, $Q_{EV} = 0$). For each panel, which corresponds to a specific cathode chemistry and charging method, the triangular coloured markers denote the EV power-voltage relationship for a given value of SoC_0 specified in the legend.

By looking at the plots, the following points can be raised.

- With CCCV charging, the active power exchange P_{EV} increases with SoC_0 . The magnitude of this trend depends on the cathode chemistry considered. Results show that LFP cells have a maximum power variation (i.e., the relative difference between the markers at $\text{SoC}_0 = 10\%$ and $\text{SoC}_0 = 90\%$) of about 5%³. This value is lower than that of other cathode chemistries ($\approx 20\%$) that behave alike due to the similarity of their OCV-SoC curves in Fig. 4.
- On the contrary, with CPCV charging, P_{EV} does not change with SoC_0 (i.e., all coloured traces are superposed on each other so that only one is visible). Moreover, the results obtained do not vary with the cathode chemistry. The only visible trend is that P_{EV} slightly decreases as the voltage v_c increases. This feature was discussed in [17], [23] and is mainly due to the power losses of the EV charger filter.

Based on the above, in the case of CPCV charging, one could fit the active power exchange P_{EV} of the EV and its CS through the EXP model of (2), which only accounts for voltage dependency. On the contrary, this expression is inadequate when considering CCCV charging due to the previously men-

³One can notice a similar power variation in Fig.2(b) of [19]. Therefore, in that paper we assume an LFP chemistry was considered for the battery pack, even though the authors do not explicitly state it.

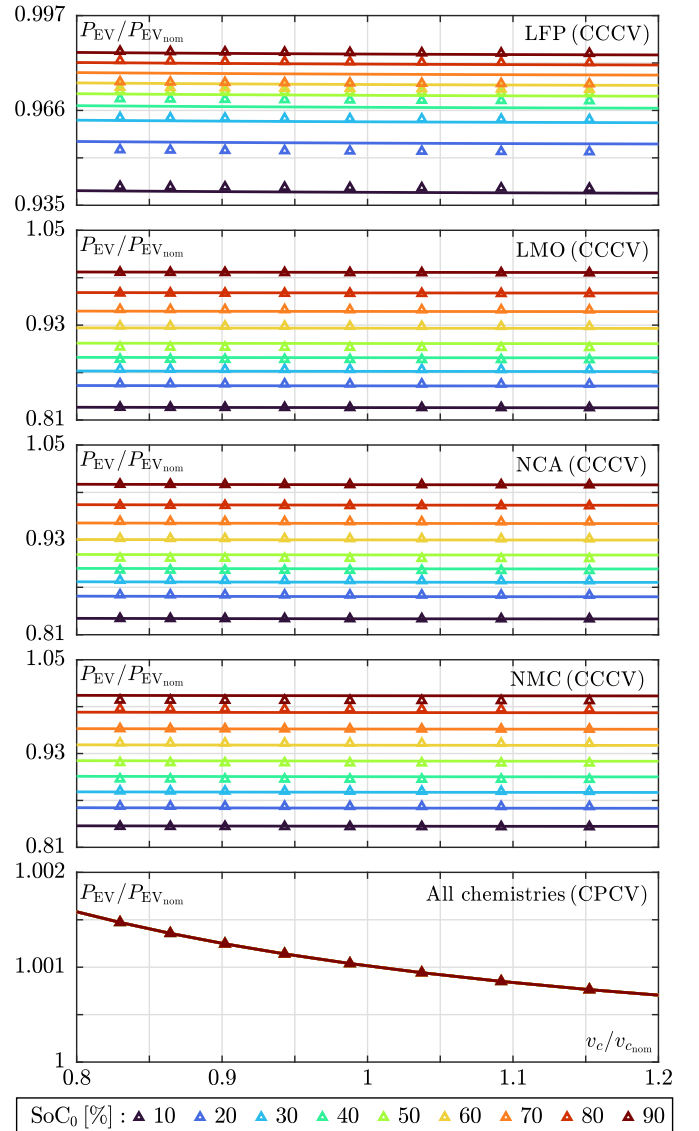


Fig. 8. Voltage-dependent active power P_{EV} (normalized w.r.t. $P_{EV,\text{nom}}$) for different cathode chemistries, charging modes, and SoC_0 values (each associated with a colour in the legend). The triangular markers correspond to the results obtained through power flow simulations and using the complete EV and CS model of section III. The solid lines are the results obtained by fitting the previous curves with (6) and (2) for CCCV and CPCV charging, respectively. Notice the reduced interval of variation of P_{EV} when the LFP chemistry is employed compared to that obtained with other cathode chemistries when CCCV charging is adopted.

tioned dependence on SOC_0 . To address this issue, some works in the literature resort to a multistage model. For instance, in [18], [19] equation (2) is still used to fit power exchange P_{EV} for different values of SOC_0 , thereby obtaining look-up tables.

In this work, instead of performing multiple fittings for each SOC_0 value, we adopted a novel and compact static model that can be intuitively derived as follows. From Fig. 3(a) and power conservation, the EV active power exchange P_{EV} is the sum of that of the AC/DC converter P_{conv} and the losses of the filter resistance R_F . In turn, assuming lossless AC/DC and DC/DC converters, by looking at Fig. 3(b) one can derive that P_{conv} equals the battery power P_{batt} . In case of constant current

charging, $P_{\text{batt}} = v_{\text{batt}} i_{\text{batt}} = N_{\text{cell,ser}} v_{\text{cell}} i_{\text{batt}}^{\text{ref}}$. Since $N_{\text{cell,ser}}$ and $i_{\text{batt}}^{\text{ref}}$ are known parameters (see Table I), the only unknown left to be determined is v_{cell} . From Fig. 3(c), neglecting for simplicity the voltage drop across the cell resistance R_{cell} , we have $v_{\text{cell}} \approx v_{\text{ocv}}$. Therefore, $P_{\text{conv}} \approx N_{\text{cell,ser}} v_{\text{ocv}} i_{\text{batt}}^{\text{ref}}$.

Based on the above, for CCCV charging, we fitted P_{EV} as

$$P_{\text{EV}} = P_{\text{EV,nom}} \left(\underbrace{b_p \left(\frac{v_c}{v_{c,\text{nom}}} \right)^{n_p}}_{V \text{ dependence}} + \underbrace{c_p - d_p \frac{1 - \text{SoC}_0}{\text{SoC}_0} + e_p e^{-f_p(1 - \text{SoC}_0)}}_{\text{SoC}_0 \text{ dependence}} \right), \quad (6)$$

where a_p , b_p , n_p , c_p , d_p , e_p , and f_p are the unknown parameters of the model. This expression includes two parts, which respectively mirror the power exchange dependence on voltage and SoC_0 . The former is primarily due to the power losses of the filter resistance R_F , which are such that P_{EV} decreases as voltage increases (i.e., $n_p < 0$) [17]. On the contrary, the latter is due to P_{conv} . As already stated and shown in Fig. 4, v_{ocv} is a function of SoC , which can be approximately described with equation (5) regardless of cathode chemistry. This suggests that similar terms can approximate P_{conv} due to its dependence on v_{ocv} . Indeed, SoC_0 dependence in (6) retraces equation (5).

The `fit` command in MATLAB was used to fit the curves in each panel of Fig. 8 with equation (6) and equation (2) for the cases based on CCCV and CPCV charging, respectively. Table II reports, for each chemistry and charging mode, the corresponding fitted parameters and root mean square error (RMSE) as an indicator of the goodness-of-fit. The solid lines in Fig. 8, colour-coded as the triangular markers, correspond to the fitted $P_{\text{EV}}/P_{\text{EV,nom}}$ results obtained in the same range of $v_c/v_{c,\text{nom}}$ and SoC_0 values. The comparison between the markers and lines, as well as the RMSE values in Table II, prove the adequacy of the fitting.

Both the static models of equation (2) and equation (6) can be easily implemented in any simulator. Moreover, they lead to a computational burden comparable to that obtained by traditionally modelling EV as constant PQ loads but, as shown in the next subsection, are more accurate.

B. Static power system studies with fleets of EVs

After analysing the active power dependency of one EV on different aspects (i.e., voltage, SoC , charging method, and cathode chemistry) and deriving a static load model, we performed static power system studies by overloading the IEEE14 network through the connection of EV fleets in parallel

to the original loads (see Fig. 7). In particular, we considered three cases where EVs and fast CSs are modelled differently.

In the first case (base case), EV fleets are represented through constant PQ loads as in most literature works. These loads do not withdraw reactive power (i.e., CSs implement active power correction), while their active power amounts to λP_{nom_i} . P_{nom_i} is the nominal power of a given load L_i (with $i \in \{1, 2, \dots, 14\}$) to which an EV fleet is connected in parallel, while λ is the overload percentage due to EV penetration, which is assumed to be 20%. To balance generation, the active power provided by the generators considered as PV busses in power flow simulations was multiplied by λ , too. Unmatched power demand is covered by the slack bus (i.e., generator G_1).

In the second case, EVs and CSs are described with the detailed model in Figs. 2–5 and employ the already mentioned different cathode cell chemistries and charging modes. In these cases, every new load added to those already existing in the benchmark consists of a fast CS to which N_{EV_i} EVs are connected in parallel. In particular, $N_{\text{EV}_i} = \text{round}(\lambda P_{\text{nom}_i} / P_{\text{EV,nom}})$, where $P_{\text{EV,nom}}$ is the nominal power of a single CS (i.e., 50 kW as stated in section III-C). The parallel connection of EVs in each CS has been synthesized through the dependent current source in the dashed section of Fig. 3(a)⁴. So doing, we assume the contemporary charge of N_{EV_i} EVs per CS.

Lastly, in the third case, EVs and CS are replaced with the static EV load models of equation (2) and equation (6) using the parameters in Table II and adequately scaling the nominal EV power $P_{\text{EV,nom}}$ to attain the same overload level λ .

Some of the results obtained by simulating the above scenarios and considering different values of SoC_0 are reported in Fig. 9 (refer to the caption for the meaning of the markers and dashed lines). The top panel shows the current flowing through the line that connects BUS1 and BUS2 (analogous trends hold for the currents in the other lines), while the bottom panel shows the total active power losses of the system.

By comparing each case, one can notice that the base one leads to the worst-case scenario (i.e., highest currents and losses). Very similar results are obtained with CPCV charge. On the contrary, with CCCV charge, lower currents and losses are obtained as smaller values of SoC_0 are considered. For example, when $\text{SoC}_0 = 10\%$, the relative percentage variation in line current (power) with respect to the base case is close to -1.6% (-2.9%) with LFP cathode chemistry, while with the other chemistries it is about -4.2% (-7.6%).

These results confirm that EVs and CSs can be adequately replaced in static power system studies by constant PQ loads when CPCV charging is used. On the contrary, with CCCV charging, this substitution becomes less acceptable as EV penetration increases and SoC_0 decreases. If so, adopting the static model in equation (6) is necessary to retain accuracy.

⁴This synthesis holds if EVs in a CS behave in the same way: this assumption suffices for the scenarios shown in this work, which only aim at validating static and dynamic EV and CS load models. A more realistic approach requires retaining the behaviour of each EV as their SoC , chemistry, charging mode, and even location could differ. However, this calls for (i) the exploitation of static and dynamic models like those presented here instead of detailed representations to limit computational burden and (ii) the addition of the probabilistic approaches mentioned in the introduction that "modulate" the N_{EV} term of this paper (which are outside the scope of this work).

TABLE II

FITTED PARAMETERS OF THE PROPOSED EV STATIC LOAD MODEL AND RMSE VALUES (IN SOME CELLS, N.A. STANDS FOR "NOT AVAILABLE").

Chemistry	a_p	b_p	n_p	c_p	d_p	e_p	f_p	RMSE
LFP (CCCV)	N.A.	0.001	-2	0.90	0.003	0.09	0.34	0.002
LMO (CCCV)	N.A.	0.001	-1.8	0.75	0.003	0.27	1.11	0.003
NCA (CCCV)	N.A.	0.001	-2.9	0.77	0.003	0.26	1.17	0.002
NMC (CCCV)	N.A.	0.001	-2	0.07	0.001	0.96	0.23	0.003
All chemistries (CPCV)	1	0.001	-2	N.A.	N.A.	N.A.	NA	$< 10^{-6}$

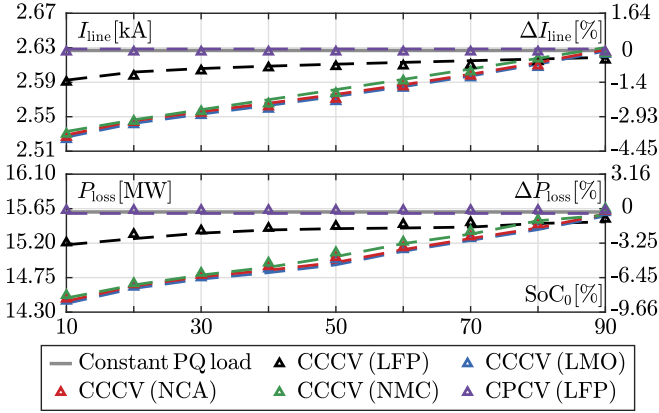


Fig. 9. Simulation results of the IEEE14 system obtained with $\lambda = 20\%$ and in the cases listed in the legend. When considering CPCV charging, only the case with LFP chemistry is reported since the other ones basically yield identical results. The results denoted by triangular markers were obtained by using the detailed model of EVs and CSs in Figs. 2–5. The solid gray line represents the results obtained by replacing the EV fleets with constant PQ loads (base case), while the dashed lines (colour-coded as the markers) represent those obtained with the static models of equation (6) and equation (2). The panels depict the line current between BUS1 and BUS2 (top) and the total active power losses (bottom) as a function of SoC_0 in physical values (left y-axis) and in relative percentage w.r.t. the base case (right y-axis).

C. Dynamic EV load model derivation

We now derive an EV dynamic load model based on VF. As in section IV-A, we considered again a single EV charged through a fast CS. To examine its dynamic behaviour during a disturbance and derive a VFLM, we simulated a -3% voltage decrease by varying the tap of the ideal transformer in Fig. 3(a). For space reasons, we discuss only the results obtained by assuming $\text{SoC}_0 = 10\%$ and adopting CPCV charging and the LFP cathode chemistry (analogous results hold for the other cases).

Figure 10 depicts the results obtained: the first two panels from the top show the magnitude and phase of $G(s)$ (derived from the detailed EV model of section III) and the relative fits of different orders derived with VF. While the first-order model is inadequate in the frequency range considered, those of order from two to three deviate from the true behaviour of $G(s)$ for frequencies higher than 10 Hz. On the contrary, the fourth-order VFLM always gives an accurate fit.

The other panels of Fig. 10 show the voltage disturbance simulated and the resulting EV active power response in the real case and for the VFLMs of different order. Other than confirming the inadequacy of the first-order model, the bottom panel highlights that increasing the VFLM order from two to four does not substantially change the accuracy of the fitted active power response. Thus, if dynamics of frequencies higher than 10 Hz are not of interest, this suggests that a second-order VFLM is enough to describe the dynamic EV behaviour.

Lastly, it is worth noting that the VFLM needs as a prerequisite accurate pre-disturbance values P_0 and v_0 (see Fig. 1 and equation (4)) [45]. As it is done here, this can be accomplished by pairing the proposed VFLM with the previously discussed static model in equation (6) or equation (2), based on the charging mode used. During power flow analyses, the static model allows deriving the correct EV steady-state operating

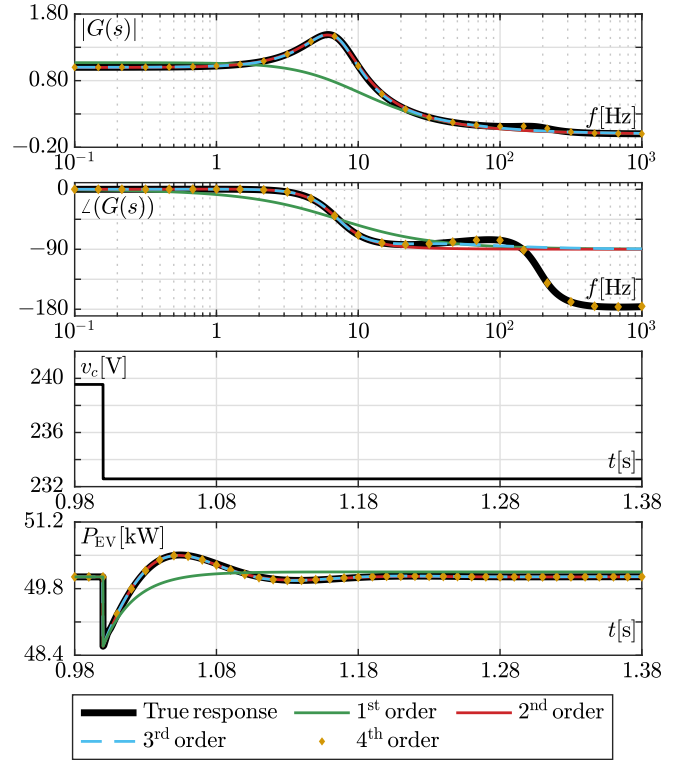


Fig. 10. First and second panel from the top: magnitude and phase, in degrees, of $G(s)$ for the detailed EV and CS model and for VFLMs of order ranging from one to four. Third and fourth panel: voltage step and corresponding EV active power response obtained in the real case and with the VFLMs.

condition and, thus, P_0 and v_0 . These values are used as input for the VFLM during small-signal or transient analyses.

D. Dynamic power system studies with fleets of EVs

Lastly, we determined the maximum amount of EVs that can be connected to the IEEE14 benchmark before instability occurs. The authors of [49] had a similar aim but described EVs with constant PQ loads. As proved in section IV-B, this simple model adequately represents EVs only in CPCV charging mode during static grid studies. However, in the case of dynamic grid studies and depending on the EV and CS converter control parameters, replacing EVs with constant PQ loads may lead to wrong results even if CPCVs charging is employed. To ensure accuracy also in these cases, dynamic load models like those described in this work are needed.

To validate these statements, we extended the work in section IV-B and swept the parameter λ across a given interval, assuming $\text{SoC}_0 = 10\%$. For each value of λ , we performed a power flow and a pole-zero analysis (i.e., stability analysis)⁵. So doing, one can derive the minimum value of λ such that the real part of at least one eigenvalue of the system switches

⁵The adoption of average EV and CS models formulated in the DQ frame is essential to perform these analyses. Indeed, it leads to the absence of harmonics, and both negative and zero sequence components. Only under these conditions, the network steady-state operation in the ABC frame corresponds to an equilibrium point in the DQ frame [50]. During pole-zero analyses, the grid model is linearized around this constant solution, thus obtaining a linear time-invariant system, whose attainment of poles and zeros is commonplace.

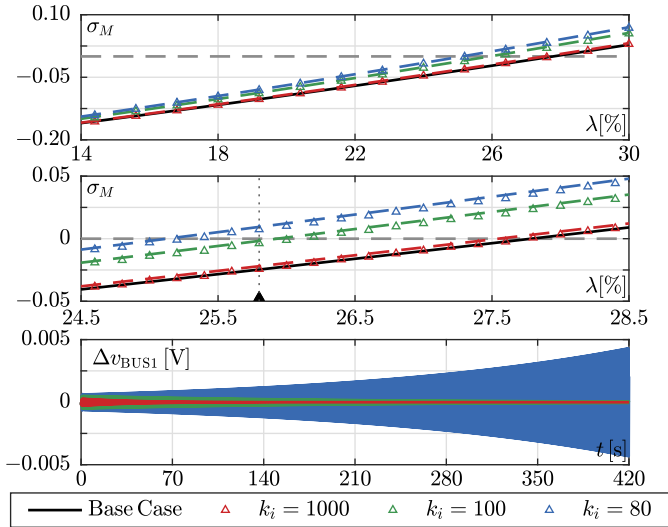


Fig. 11. Top panel: maximum real part σ_M of the eigenvalues of the modified IEEE14 system obtained by sweeping λ from 14% to 30% and considering the k_i values of the PI₁ regulator shown in the legend. The gray dashed line is placed at $\sigma_M = 0$. The triangular markers show the results obtained with the detailed EV and CS model in Figs. 2–5. The solid black line represents the results obtained by replacing EV fleets with constant PQ loads, while the dashed lines represent those achieved with the second-order VFLM of section IV-C. The middle panel is an inset of the top panel. Bottom panel: voltage deviations at BUS1 around its steady-state value due to a load disturbance, obtained for different values of k_i and $\lambda = 25.8\%$.

from negative to positive (i.e., instability occurs). For brevity, we discuss only the results obtained with CPCV charging and the LFP cathode chemistry. As in section IV-B, we considered three cases, each corresponding to a different EV and fast CS model. In the first case, we adopted the accurate model of Figs. 2–5. In the second case, constant PQ loads replace the fleet of EVs. Lastly, in the third case we adopted the second-order VFLM of section IV-C. Moreover, we analysed how results change when the parameter k_i of the regulator PI₁ equals 1000, 100, and 80 (in each case, the VFLM parameters were updated to ensure a proper fit). The reason for this was twofold: first, to exemplify the impact of the tuning of converter controls in EVs and CSs on grid stability; second, to highlight the accuracy of the proposed dynamic model.

The top and middle panel of Fig. 11 show how the maximum real part of the eigenvalues of the IEEE14 benchmark evolve in a given range of λ for each case (refer to the caption for the meaning of the markers and the solid and dashed lines). These panels highlight two aspects. First, based on the control parameters in Fig. 5, constant PQ loads may not adequately reflect the true behaviour of EVs and CSs, and not even lead to the worst-case scenario. Indeed, as k_i decreases, the pole-zero analysis results obtained by replacing EV fleets with PQ loads increasingly differ from the true ones⁶. Second, the very good match between the triangular markers and dashed lines of the same colour proves that the proposed second-order

⁶If CCCV charging were considered, instability would occur for values of λ higher than those obtained with CPCV charging and shown in Fig. 11. This happens because, for the same value of λ , the actual level of stress in the grid (e.g., higher currents and grid losses) due to EV fleets is generally lower with CCCV than CPCV charging, regardless of SoC₀. This feature, which can be observed in Fig. 9, translates into higher stability margins.

VFLM can correctly replace detailed EV and fast CS models in stability studies, regardless of the tuning of their converter control parameters.

As a further proof of the results obtained with the pole-zero analyses, we performed transient simulations of the modified IEEE14 benchmark by assuming $\lambda = 25.8\%$ (black arrowhead in the middle panel of Fig. 11) and considering the previous values of k_i . Based on the pole-zero analysis and the above value of λ , the case with $k_i = 80$ is unstable, whereas those with $k_i = 100$ and 1000 lead to a stable system (indeed, for $\lambda = 25.8\%$, only in the first case there is at least one pole with positive real part). This is confirmed by the bottom panel of Fig. 11, which shows the voltage deviations at BUS 1 around its steady-state value after a small load disturbance. As expected, only when $k_i = 80$ are voltage oscillations not damped: in fact, they diverge rather slowly because for $\lambda = 25.8\%$ the positive real part of the unstable pole is close to zero⁷.

V. CONCLUSIONS

We have presented accurate and computationally efficient static and dynamic load models for EVs and fast CSs, which take into account the dependence of active power exchange on voltage, SoC, charging method, cathode chemistry, and converter controls. These models can replace the standard EV representation as constant PQ loads to assess more reliably the impacts of electric mobility during static and dynamic grid studies. Through the simulation results of the IEEE14 benchmark, we have validated the accuracy of the proposed models and highlighted that in some cases the standard EV representation as constant PQ loads lacks accuracy.

In particular, we have shown that, when CCCV charging is employed, the battery cathode chemistry and SoC significantly affect EV power exchange. This behaviour cannot be adequately mimicked through constant PQ loads. Moreover, due to the EV and CS control system parameters, this simplified representation may not adequately reflect the dynamic behaviour of EVs, even if CPCV charging is used.

REFERENCES

- [1] “Global EV Outlook 2022: Securing supplies for an electric future,” <https://www.iea.org/reports/global-ev-outlook-2022>.
- [2] S. Habib, M. M. Khan, F. Abbas, L. Sang, M. U. Shahid, and H. Tang, “A comprehensive study of implemented international standards, technical challenges, impacts and prospects for electric vehicles,” *IEEE Access*, vol. 6, pp. 13 866–13 890, 2018.
- [3] M. Nour, J. P. Chaves-Ávila, G. Magdy, and A. Sánchez-Miralles, “Review of positive and negative impacts of electric vehicles charging on electric power systems,” *Energies*, vol. 13, no. 18, p. 4675, Sep 2020.
- [4] A. Arias-Londoño, O. D. Montoya, and L. F. Grisales-Noreña, “A chronological literature review of electric vehicle interactions with power distribution systems,” *Energies*, vol. 13, no. 11, p. 3016, Jun 2020.
- [5] G. R. Chandra Mouli, M. Kefayati, R. Baldick, and P. Bauer, “Integrated PV charging of EV fleet based on energy prices, V2G, and offer of reserves,” *IEEE Trans. Smart Grid*, vol. 10, no. 2, pp. 1313–1325, 2019.
- [6] N. H. Tehrani and P. Wang, “Probabilistic estimation of plug-in electric vehicles charging load profile,” *Electr. Pow. Syst. Res.*, vol. 124, pp. 133–143, 2015.

⁷It is also worth pointing out that the voltage oscillations obtained in the unstable case for $k_i = 80$ have a frequency lower than 10 Hz, which justifies the adequacy of adopting a second-order VFLM. If that were not the case, based on what was stated in section IV-C, a higher order should be used.

- [7] J. C. Mukherjee and A. Gupta, "A review of charge scheduling of electric vehicles in smart grid," *IEEE Syst. J.*, vol. 9, no. 4, pp. 1541–1553, 2015.
- [8] B. Wang, D. Zhao, P. Dehghanian, Y. Tian, and T. Hong, "Aggregated electric vehicle load modeling in large-scale electric power systems," *IEEE Trans. Ind. Appl.*, vol. 56, no. 5, pp. 5796–5810, 2020.
- [9] J. V. Milanovic, K. Yamashita, S. Martínez Villanueva, S. v. Djokic, and L. M. Korunović, "International industry practice on power system load modeling," *IEEE Trans. Power Syst.*, vol. 28, no. 3, pp. 3038–3046, 2013.
- [10] D. del Giudice, F. Bizzarri, S. Grillo, D. Linaro, and A. M. Brambilla, "Impact of passive-components' models on the stability assessment of inverter-dominated power grids," *Energies*, vol. 15, no. 17, p. 6348, Aug 2022.
- [11] I. Pasiopoulou, E. Kontis, T. Papadopoulos, and G. Papagiannis, "Effect of load modeling on power system stability studies," *Electr. Pow. Syst. Res.*, vol. 207, p. 107846, 2022.
- [12] A. M. A. Haidar and K. M. Muttaqi, "Behavioral characterization of electric vehicle charging loads in a distribution power grid through modeling of battery chargers," *IEEE Trans. Ind. Appl.*, vol. 52, no. 1, pp. 483–492, 2016.
- [13] J. Gil-Aguirre, S. P.-L. no, and J. Mora-Flórez, "A measurement-based load modelling methodology for electric vehicle fast-charging stations," *Electr. Pow. Syst. Res.*, vol. 176, p. 105934, 2019.
- [14] A. Haidar, K. Muttaqi, and M. Haque, "Multistage time-variant electric vehicle load modelling for capturing accurate electric vehicle behaviour and electric vehicle impact on electricity distribution grids," *IET Generation, Transmission & Distribution*, vol. 9, 09 2015.
- [15] E. Sortomme, A. I. Negash, S. S. Venkata, and D. S. Kirschen, "Multistate voltage dependent load model of a charging electric vehicle," in *2012 IEEE Transportation Electrification Conference and Expo (ITEC)*, 2012, pp. 1–5.
- [16] —, "Voltage dependent load models of charging electric vehicles," in *2013 IEEE Power & Energy Society General Meeting*, 2013, pp. 1–5.
- [17] C. Dharmakeerthi, N. Mithulananthan, and T. Saha, "Impact of electric vehicle fast charging on power system voltage stability," *Int. J. Electr. Power Energy Syst.*, vol. 57, pp. 241–249, 2014.
- [18] A. Shukla, K. Verma, and R. Kumar, "Multi-stage voltage dependent load modelling of fast charging electric vehicle," in *2017 6th International Conference on Computer Applications In Electrical Engineering-Recent Advances (CERA)*, 2017, pp. 86–91.
- [19] —, "Voltage-dependent modelling of fast charging electric vehicle load considering battery characteristics," *IET Electrical Systems in Transportation*, vol. 8, no. 4, pp. 221–230, 2018.
- [20] F. Islam, H. Pota, M. A. Mahmud, and M. Hossain, "Impact of PHEV loads on the dynamic performance of power system," in *2010 20th Australasian Universities Power Engineering Conference*. IEEE, 2010, pp. 1–5.
- [21] C. Dharmakeerthi, N. Mithulananthan, and T. Saha, "Impact of electric vehicle load on power system oscillatory stability," in *2013 Australasian Universities Power Engineering Conference (AUPEC)*. IEEE, 2013, pp. 1–6.
- [22] C. Dharmakeerthi, N. Mithulananthan, and A. Atputharajah, "Development of dynamic EV load model for power system oscillatory stability studies," in *2014 Australasian Universities Power Engineering Conference (AUPEC)*. IEEE, 2014, pp. 1–6.
- [23] H. Tian, D. Tzelepis, and P. N. Papadopoulos, "Electric vehicle charger static and dynamic modelling for power system studies," *Energies*, vol. 14, no. 7, p. 1801, Mar 2021.
- [24] T. Ioannis, T. Dalius, and L. Natalia, "Li-ion batteries for mobility and stationary storage applications," 2018.
- [25] P. H. Camargos, P. H. J. dos Santos, I. R. dos Santos, G. S. Ribeiro, and R. E. Caetano, "Perspectives on li-ion battery categories for electric vehicle applications: A review of state of the art," *International Journal of Energy Research*, vol. 46, no. 13, pp. 19258–19268, 2022.
- [26] G. A. Barzegkar-Ntovom, E. O. Kontis, T. A. Papadopoulos, and P. N. Papadopoulos, "Methodology for evaluating equivalent models for the dynamic analysis of power systems," *IEEE Trans. Power Del.*, vol. 37, no. 6, pp. 5059–5070, 2022.
- [27] L. M. Korunović, J. V. Milanović, S. Z. Djokic, K. Yamashita, S. M. Villanueva, and S. Sterpu, "Recommended parameter values and ranges of most frequently used static load models," *IEEE Trans. Power Syst.*, vol. 33, no. 6, pp. 5923–5934, 2018.
- [28] A. Kurita and T. Sakurai, "The power system failure on July 23, 1987 in Tokyo," in *Proceedings of the 27th IEEE Conference on Decision and Control*, 1988, pp. 2093–2097 vol.3.
- [29] K. P. Schneider, J. C. Fuller, and D. P. Chassin, "Multi-state load models for distribution system analysis," *IEEE Trans. Power Syst.*, vol. 26, no. 4, pp. 2425–2433, 2011.
- [30] D. Hill, "Nonlinear dynamic load models with recovery for voltage stability studies," *IEEE Trans. Power Syst.*, vol. 8, no. 1, pp. 166–176, 1993.
- [31] E. O. Kontis, T. A. Papadopoulos, A. I. Chrysochos, and G. K. Papagiannis, "Measurement-based dynamic load modeling using the fitting technique," *IEEE Trans. Power Syst.*, vol. 33, no. 1, pp. 338–351, 2018.
- [32] E. S. N. R. Paidi, A. Nechifor, M. M. Albu, J. Yu, and V. Terzija, "Development and validation of a new oscillatory component load model for real-time estimation of dynamic load model parameters," *IEEE Trans. Power Del.*, vol. 35, no. 2, pp. 618–629, 2020.
- [33] B. Gustavsen and A. Semlyen, "Rational approximation of frequency domain responses by vector fitting," *IEEE Trans. Power Del.*, vol. 14, no. 3, pp. 1052–1061, 1999.
- [34] B. Gustavsen, "Improving the pole relocating properties of vector fitting," *IEEE Trans. Power Del.*, vol. 21, no. 3, pp. 1587–1592, 2006.
- [35] D. Deschrijver, M. Mrozowski, T. Dhaene, and D. De Zutter, "Macro-modeling of Multiport Systems Using a Fast Implementation of the Vector Fitting Method," *IEEE Microw. Wireless Compon. Lett.*, vol. 18, no. 6, pp. 383–385, 2008.
- [36] "Vector fitting Website - download page of the vector fitting package," <https://www.sintef.no/projectweb/vectorfitting/downloads/>, last update: 2013.
- [37] G. L. Plett, *Battery management systems, Volume II: Equivalent-circuit methods*. Artech House, 2015.
- [38] M. Restrepo, J. Morris, M. Kazerani, and C. A. Canizares, "Modeling and testing of a bidirectional smart charger for distribution system EV integration," *IEEE Trans. Smart Grid*, vol. 9, no. 1, pp. 152–162, 2016.
- [39] G. L. Plett, *Battery management systems, Volume I: Battery modeling*. Artech House, 2015.
- [40] O. Tremblay and L.-A. Dessaint, "Experimental validation of a battery dynamic model for EV applications," *World Electric Vehicle Journal*, vol. 3, no. 2, p. 289–298, Jun 2009.
- [41] J. P. Fernández-Porrás, S. Grillo, F. D'Agostino, and F. Silvestro, "Mitigation of voltage deviations in DC shipboard microgrids through the active utilization of battery energy storage systems," in *2018 IEEE Power & Energy Society General Meeting (PESGM)*, 2018, pp. 1–5.
- [42] M.-K. Tran, A. DaCosta, A. Mevawalla, S. Panchal, and M. Fowler, "Comparative study of equivalent circuit models performance in four common lithium-ion batteries: LFP, NMC, LMO, NCA," *Batteries*, vol. 7, no. 3, p. 51, 2021.
- [43] A. Yazdani and R. Iravani, *Voltage-sourced converters in power systems: modeling, control, and applications*. John Wiley & Sons, 2010.
- [44] J. A. Sanguesa, V. Torres-Sanz, P. Garrido, F. J. Martinez, and J. M. Marquez-Barja, "A review on electric vehicles: Technologies and challenges," *Smart Cities*, vol. 4, no. 1, p. 372–404, Mar 2021.
- [45] F. Milano, *Power System Modelling and Scripting*, ser. Power systems. Springer, 2010.
- [46] F. Bizzarri, A. Brambilla, G. S. Gajani, and S. Banerjee, "Simulation of Real World Circuits: Extending Conventional Analysis Methods to Circuits Described by Heterogeneous Languages," *IEEE Circuits Syst. Mag.*, vol. 14, no. 4, pp. 51–70, Fourthquarter 2014.
- [47] F. Bizzarri and A. Brambilla, "PAN and MPanSuite: Simulation Vehicles towards the Analysis and Design of Heterogeneous Mixed Electrical Systems," in *NGCAS*. IEEE, 2017, pp. 1–4.
- [48] D. Linaro, D. del Giudice, F. Bizzarri, and A. Brambilla, "Pansuite: A free simulation environment for the analysis of hybrid electrical power systems," *Electr. Pow. Syst. Res.*, vol. 212, p. 108354, 2022.
- [49] M. Moschella, M. A. A. Murad, E. Crisostomi, and F. Milano, "On the impact of PEV charging on transmission system: Static and dynamic limits," in *2020 IEEE Power & Energy Society General Meeting (PESGM)*, 2020, pp. 1–5.
- [50] F. Bizzarri, D. del Giudice, D. Linaro, and A. Brambilla, "Numerical approach to compute the power flow solution of hybrid generation, transmission and distribution systems," *IEEE Trans. Circuits Syst. II*, vol. 67, no. 5, pp. 936–940, 2020.